Intelligent Tuning of Commutation for Maximum Torque Capability of a Switched Reluctance Motor

K. I. Hwu and C. M. Liaw, *Member, IEEE*

***Abstract*—Since the winding current and inductance profiles of a switched reluctance motor (SRM) are far from ideal, its torque generating characteristics are quite ambiguous and difficult to optimize quantitatively. In this paper, the intelligent commutation tuning control to improve the torque generating performance of an SRM is presented. First, the effect of the commutation instant on the torque characteristics of a singly excited SRM is observed. Then accordingly, an intelligent method of commutation tuning is developed to improve the torque generating capability. In making the tuning, the minimization of the motor drawn line current is employed as a performance index to equivalently yield maximum torque per ampere (TPA). Finally, the circuit implementation of the developed tuning scheme is carried out. The appropriate commutation makes the motor draw minimum current under any load condition. It follows that the motor conversion efficiency is also improved. In addition, owing to the increased torque generating capability, the tracking and regulation speed control performances are also improved. Some experimental results are provided to demonstrate the effectiveness of the proposed control scheme.**

***Index Terms*—Commutation control, current minimization, efficiency maximization, switched reluctance motor.**

NOMENCLATURE

B, J	Damping ratio and inertia moment.
$d = v_c/\hat{V}_{saw}$	PWM duty ratio.
$e_n(i_n, \theta_r)$	Phase-winding back electromotive force.
$G_{c\omega}(s) = k_{p\omega} + k_{i\omega}/s$	Speed feedback controller.
$G_{ci}(s) = k_{pi} + k_{ii}/s$	Current feedback controller.
$H_n(s)$	Phase closed-loop current-tracking transfer function.
I_c	Current command magnitude.
i_n, i_{cn}	Phase-winding current and its command.
K	Proportional gain employed to adjust control sensitivity.
k_t	Torque generating function.
L_a, L_u	Aligned and unaligned position inductances.
$L_n(i_n, \theta_r)$	Phase-winding incremental inductance.
$P_1 \sim P_4$	Switching signals decopuled from Hall sensor outputs.
p_{dn}	Developed power of nth phase winding.
$Q_n, \bar{Q}_n$	Phase-delayed signal and its complementary.
R	Stator phase-winding resistance.
R_L	Load resistance.
R_{sw}	Turn-on resistance of the CMOS switch.
R_v	Variable resistance used in the timing network of SN74121.
R_1, R_2	Resistances to represent part of R_v.
$S_1 \sim S_4$, $T_1 \sim T_4$	Switches used in the lower and upper parts of converter legs.
T_{dn}	nth phase winding developed torque
T_e	Total developed torque.
T_L	Load torque.
$\hat{V}_{saw}$	Amplitude of v_{saw}.
v_c	Control voltage.
v_{saw}	Sawtooth voltage.
$\lambda_n(i_n, \theta_r)$	nth phase flux linkage.
θ_d, θ_{on}, θ_{off}	Dwell angle, turn-on angle, and turn-off angle.
θ_r	Rotor angular position.
ω_r, ω_r^*,	Rotor angular speed and its command.
τ	Turn-on period of commutation timing signal.
$\tau_1 = R_v C$	Delay time interval.
$\tau_2 = \tau - \tau_1$	Advancing duration.
$(\cdot)(n)$	Value of $(\cdot)$ at nth sampling interval.
$\Delta(\cdot)$	Small change of $(\cdot)$.

Manuscript received September 5, 2000; revised November 13, 2001. This research was supported by the National Science Council of R.O.C. under Grant NSC 89-2213-E-007-072.

The authors are with the Department of Electrical Engineering, National Tsing Hua University, Hsinchu, Taiwan, R.O.C. (e-mail: cmliaw@ee.nthu.edu.tw).

Digital Object Identifier 10.1109/TEC.2002.808406

I. INTRODUCTION

IN ADDITION to some structural advantages, the switched reluctance motor (SRM) also possesses remarkable features in its converter such as [1]: simple circuit configuration, freedom from shoot-through fault, and ease of switching control. However, the SRM suffers from some disadvantages and until now, a lot of research has been done to improve its operating performance. This includes converter circuit improvement [3],[4]; dc-link voltage boosting [5], [6], advancing commutation [7]–[16] in current switching control; motor design; acoustic noise reduction; small-signal dynamic modeling; and sophisticated speed control methods.

Physically, the torque generating characteristics of the SRM depend heavily on whether the phase current is in accordance with the inductance variation feature. Hence, the actual phase current profile plays an important role in the torque producing capability and basically there are three tunable variables: 1) current waveform; 2) turn-on angle θ_{on}; and 3) turn-off angle θ_{off}. And the performance indices usually used for making performance evaluation are conversion efficiency, torque ripple,

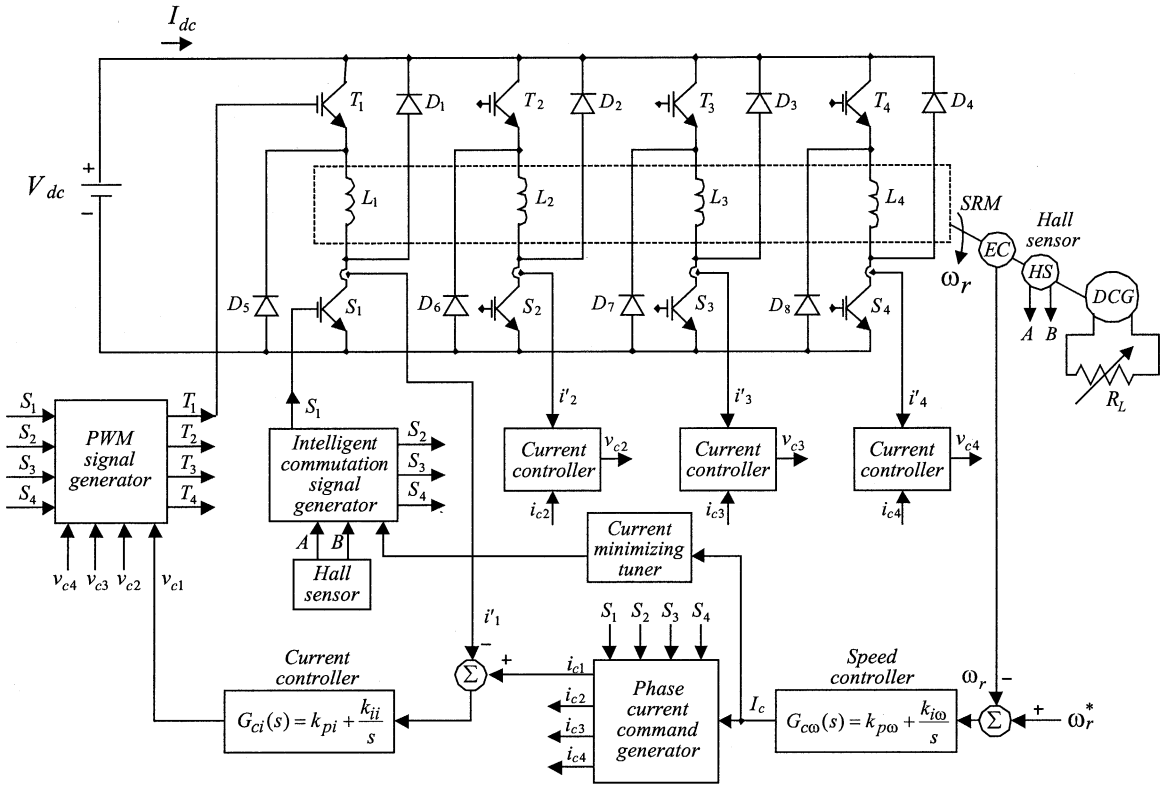

Fig. 1. System configuration of the experimental SRM drive.

or torque per ampere (TPA). During the past years, several researches in switching control have been made, for example, the control of acquiring maximum motor drive efficiency [7]; the torque ripple minimization [8], [9]; and the current waveforms generated for maximum torque per root-mean-square (rms) ampere [10]. As to the studies in the commutation instant tuning, some online self-tuning algorithms have been presented, including θ_{on} altered and θ_{off} fixed [12], [15], or θ_{on} fixed and θ_{off} altered [12]–[16]. Most of them focus on the tuning control of the multiply-excited SRM but few on the singly excited SRM. The self-tuning method developed in [12] uses a steady-state speed-dependent algorithm to alter turn-on angle for minimizing the dc-link power. The measured results indicated that the searching convergent speed is slow. As to the self-tuning technique presented in [13], a simple algorithm along with a lookup table is used to optimize the TPA with additional computer simulation proving its existence and uniqueness. Concerning the optimization of the TPA made in [14] and [15], the artificial neural networks (ANNs) are applied to perform the online self-tuning of turn-on or turn-off angle. However, a lot of simulated or measured data are required for training and establishing the NNs. And as to the self-tuning controller in [16], online identification is used for adjusting the turn-off angle to minimize the torque ripple.

It is known that the torque generating characteristic of an SRM drive is significantly affected by the inductance and current profiles and it is very difficult to directly control since the torque information is normally not directly available. Thus in this paper, the improvement of torque generating performance of the SRM via intelligent tuning is studied. Initially, the effect of commutation instant variation on the torque characteristics of a singly excited SRM is observed intuitively. Subsequently, an intelligent commutation tuning approach is developed to optimize the torque producing capability. Intuitively, the larger torque the motor is generated, the less the current is drawn. Therefore, in performing the tuning, the minimization of winding current command, and hence, motor drawn line current is employed as a performance index. Finally, the circuit implementation of the proposed tuning scheme is made to stably achieve the desired control performance. The developed intuitive searching control algorithm is simple, no motor model and parameters are required. Moreover, the simulation and measured data are also not necessary for developing the proposed searching control algorithm. The appropriate commutation made by the proposed approach can let the motor drawn current be minimum under any load condition. And accordingly, the speed dynamic responses are also improved. The control performances are insensitive to the variations of system operation conditions and parameters. Effectiveness of the proposed strategy is verified by some experimental results.

II. Configuration of the Proposed SRM Drive

The configuration of the proposed SRM drive is shown in Fig. 1. It consists of an SRM with an encoder (EC) and a Hall-effect sensor (HS), a converter circuit, a proportional-plus-integral (PI) speed controller $G_{c\omega}(s)$, a phase winding current command generator, four PI winding current controllers $G_{ci}(s)$, a PWM signal generator, the proposed current minimizing tuner and intelligent commutation signal generator, and a permanent dc generator having variable load resistance R_L. The generator is mechanically coupled on to the motor to serve as its dynamic load.

As to the current commands of the winding current controllers, their commutation instants are first roughly set according to the sensed rotor position information, then they are adjusted by the current minimizing tuner to achieve the desired performance.

The SRM employed in this experimental drive system is manufactured by the TASC Drives Ltd., U.K., and it is 8/6 poles, four-phase, 4.4 kW, 1500 r/min.

Suppose the SRM is singly excited and the hysteresis of magnetic circuit is neglected, the terminal voltage of phase 1 winding is given by

$$\begin{aligned} v_1 =& Ri_1 + \frac{d\lambda_1(i_1,\theta_r)}{dt} \\ =& Ri_1 + \frac{\partial\lambda_1(i_1,\theta_r)}{\partial i_1}\frac{di_1}{dt} + \frac{\partial\lambda_1(i_1,\theta_r)}{\partial\theta_r}\frac{d\theta_r}{dt} \\ \triangleq& Ri_1 + L_1(i_1,\theta_r)\frac{di_1}{dt} + k_t(i_1,\theta_r)\omega_r \\ \triangleq& Ri_1 + L_1(i_1,\theta_r)\frac{di_1}{dt} + e_1(i_1,\theta_r) \end{aligned} \tag{1}$$

where v_1 is the terminal voltage; R is the phase-winding resistance; $\theta_r =$ is the rotor angular position; $\omega_r = d\theta_r/dt =$ is the rotor angular speed; $\partial\lambda_1(i_1,\theta_r)/\partial i_1 = L_1(i_1,\theta_r) =$ is the phase-winding incremental inductance; $\partial\lambda_1(i_1,\theta_r)/\partial\theta_r = k_t(i_1,\theta_r) =$ is the coefficient of equivalent back emf $e_1(i_1,\theta_r) = k_t(i_1,\theta_r)\omega_r =$ equivalent back emf.

The developed power and torque generated by phase 1 winding can be found as

$$p_{d1}(t) = e_1(i_1,\theta_r)\,i_1 = k_t(i_1,\theta_r)\,\omega_r i_1 \tag{2}$$

and

$$T_{d1} = \frac{p_{d1}}{\omega_r} = k_t(i_1,\theta_r)\,i_1 \tag{3}$$

Similar terminal voltage and generated torque equations for other three phase windings can also be derived. Then one can obtain the following torque equation:

$$T_e = \sum_{i=1}^{4} T_{di} = T_L + B\omega_r + J\frac{d\omega_r}{dt} \tag{4}$$

where T_e is the sum of the torque developed by all phases with mutual inductance effect neglected; T_L is the load torque; and J and B denote the total moment of inertia and the damping ratio, respectively.

Observations:

i) Equation (1) implies that the winding excitation current tracking response is remarkably affected by the inductance and the back emf, which both dependent on the position/speed and the excitation current level. At higher speed, the back emf will be a dominant factor.

ii) Equations (3) and (4) indicate that the transfer function block diagram drawn in Fig. 2 can be used to represent the dynamic behavior of the SRM drive shown in Fig. 1,where $H_n(s)(n = 1 \sim 4)$ denotes the closed-loop current tracking transfer function. But due to the existence of the nonlinear inductance and back emf, $H_n(s)$ is far from ideal (*i.e.*, $H_n(s) = 1$). The higher the rotor speed is, the more the current response deviates from ideal. The nonlinear feature of the torque generating function k_t of each phase can be known from (1).

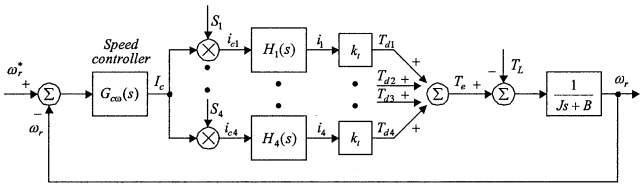

Fig. 2. Control system block diagram of the SRM drive.

III. Proposed Tuning Scheme

A. Intuitive Analysis and Problem Statement

It is obvious from the above observations that the electromagnetic (EM) torque generating behavior, which is a nonlinear function of motor parameters and current, is quite chaotic. For the convenience of developing the proposed self-tuning approach, the effect of commutation instant variation on the torque generating characteristics of an SRM is observed intuitively. For ease of analyzing the developed torque generated according to winding inductance profiles and winding current waveforms, the following assumptions are made

i) the SRM is singly excited;

ii) the phase inductance is independent of current level and represented by a trapezoid as a function of position, in which L_a and L_u denote the winding inductance at aligned and unaligned positions, respectively;

iii) the phase current waveform is approximately expressed by a trapezoid.

On the bases of (i) and (ii), the developed torque can be calculated by using the following formula with the mutual inductance being neglected:

$$T_e = \sum_{n=1}^{4} \frac{1}{2} i_n^2 \frac{dL_n}{d\theta_r}. \tag{5}$$

The developed torque for the assumed current profiles without commutation advancing is sketched in Fig. 3(a). One can find that due to the nonideal current response, the resultant torque is no longer ripple free and with a less average value. In light of this, the turn-on and turn-off angles are shifted forward as shown in Fig. 3(b). This causes both the average torque and ripple torque to be increased. However, the excessive advance of the commutation instant may lead to the decrease of average torque.

In actual operations, the torque generated by an SRM is more complicated and difficult to handle, as described in Section II. This is attributed to the following facts: 1) the winding inductance is also a nonlinear function of current level and it is bell shaped rather than the trapezoid shown in Fig. 3(a) and (b); and 2) the waveform of winding current is considerably affected by the variations of the motor inductance and the back emf.

Proposed Control Methodology: The conceptual block diagram for explaining the proposed tuning control methodology is drawn in Fig. 3(c), wherein the typical PWM switching-controlled winding current waveforms without and with commutation advancing are also sketched. Similar to the observations made in Fig. 3(a) and (b), one can also find that both the average and ripple torque characteristics are much affected by the change of commutation instant. For many

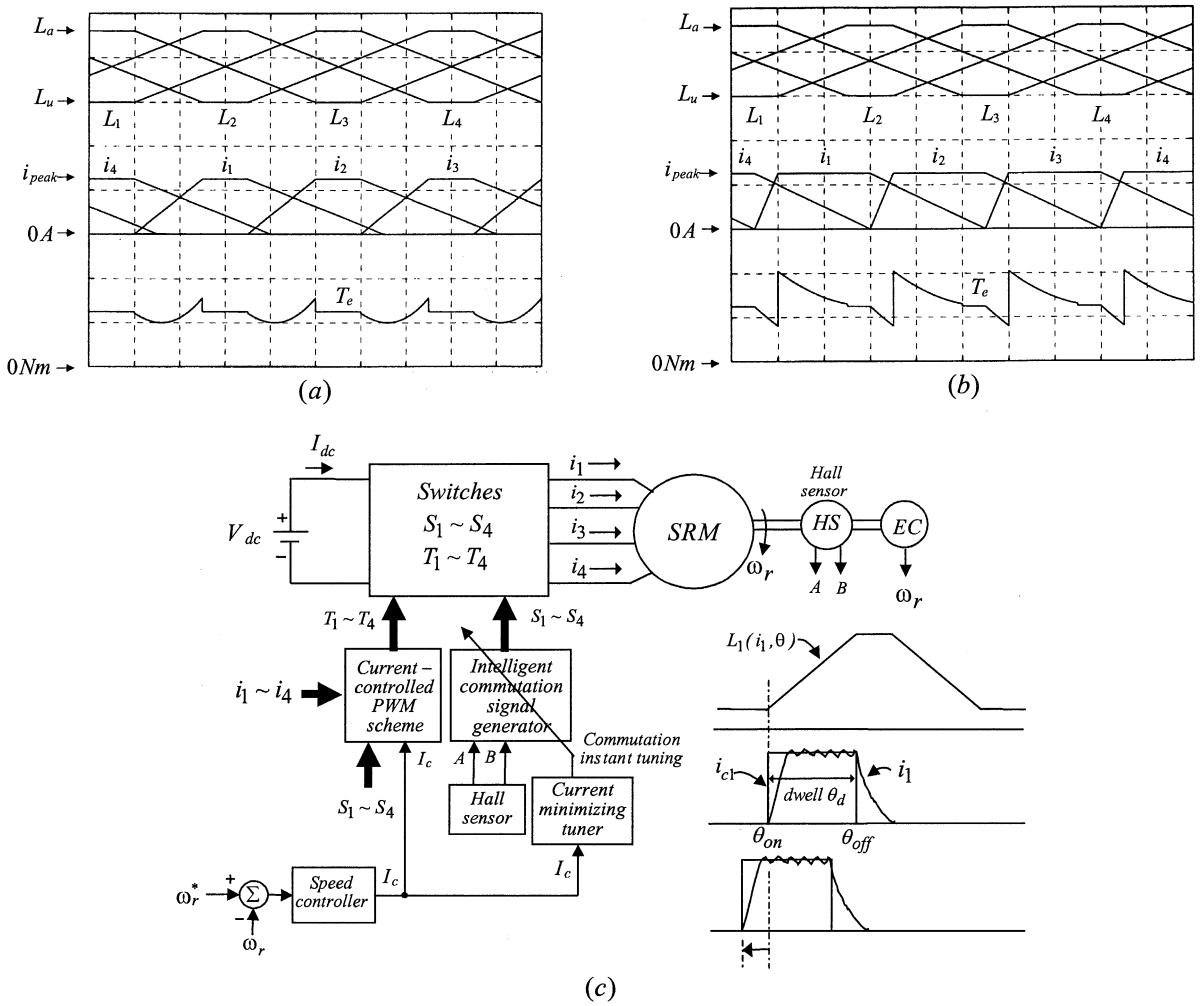

Fig. 3. (a) Developed torque without commutation advancing; (b) developed torque with commutation advancing; (c) conceptual block diagram for explaining the proposed tuning control methodology.

applications where their mechanical time constants are not too small, the torque ripple is less important. And intuitively, the larger average torque the motor is generated, the less the current will be drawn for a particular load. Therefore, in the proposed tuning control scheme, the turn-on and turn-off angles are adjusted with the motor drawn line current minimization being employed as a performance index.

B. Proposed Intelligent Commutation Signal Generator

Fig. 4 shows the configuration of the proposed intelligent commutation signal generating scheme and its typical waveforms are sketched in Fig. 5, which are used to explain the detailed procedure for generating the advancing commutation timing signals. In Figs. 4(a) and 5, the original commutation timing signals P_1, P_2, P_3, and P_4 are decoupled from two-phase position sensor signals A and B and the delayed signals $Q_i(i = 1 \sim 4)$ are yielded through the TTL IC *SN*74 121. The delay time τ_1 is determined by the variable resistance R_v, which is varied using pulse-width-modulation (PWM) control technique based on the proposed tuning algorithm. The PWM controlled scheme for yielding variable resistance will be introduced in detail later. According to the circuit shown in Fig. 4(a), the ith modified commutation timing signal S_i can be obtained by

$$\begin{aligned} S_i =& (Q_{i-1} \cap \bar{P}_i \cap \bar{P}_{i+1} \cap \bar{P}_{i+2}) \cup \bar{Q}_i, i = 1 \sim 4 \\ &\text{if } i-1 = 0, \text{ then } i-1 \triangleq 4 \\ &\text{if } i+1 > 4 \text{ or } i+2 > 4, \text{ then } i+1 \triangleq i-3 \text{ or} \\ &\quad i+2 \triangleq i-2 \end{aligned} \tag{6}$$

where $\cap$ and $\cup$ denote the ANDed and the ORed processes, respectively. For example, if $i = 4$, then

According to (6), the resulted modified and original commutation signals are sketched in Fig. 5. The results in Fig. 5 indicate that the modified commutation timing signals $S_i(i = 1 \sim 4)$ lead the original ones $P_i(i = 1 \sim 4)$ by a duration τ_2, which can be adjusted via the change of τ_1, according to the following relationship:

$$\tau_2 = \tau - \tau_1, \tau_1 = R_v C \tag{7}$$

where τ_1 is the delay time interval determined by *SN*74121, R_v and C are the timing network of *SN*74 121, and τ denotes the turn-on period of the commutation timing signal. This corre-

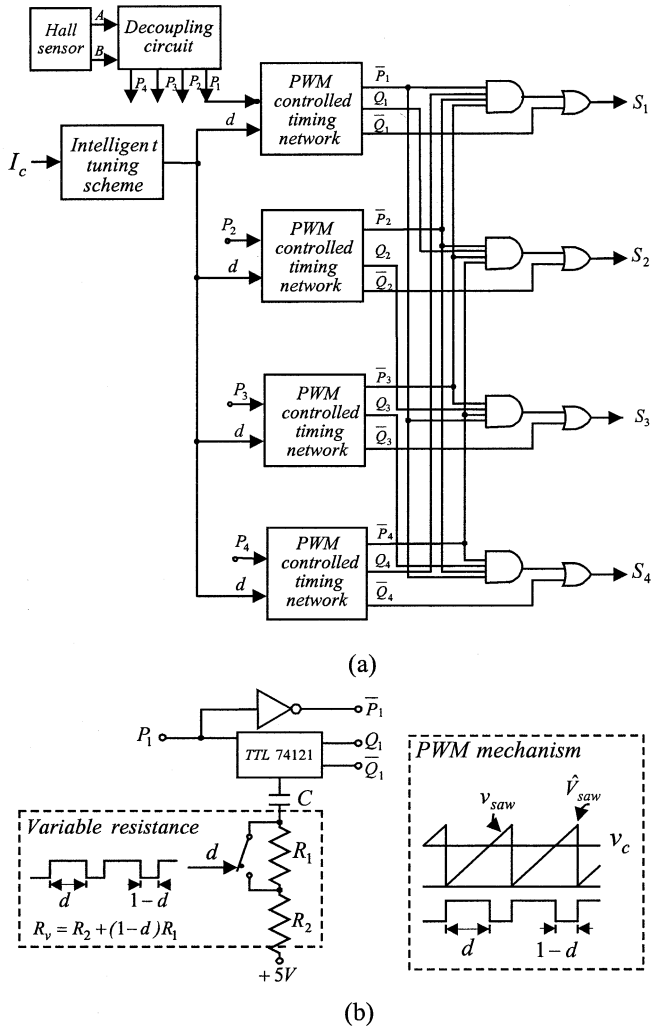

Fig. 4. Configuration of the proposed intelligent commutation signal generating scheme: (a) advancing signal generating circuits; (b) PWM controlled timing network to control the delay time of the monostable multivibrator.

sponds to that the turn-on angle θ_{on} is advanced by an angle of $\tau_2\omega_r$ and the dwell angle is equal to $\theta_d = \tau\omega_r$.

C. PWM-Controlled Timing Network

A PWM-controlled timing network to control the delay time of the monostable multivibrator integrated circuit (IC) *SN*74 121 is shown in Fig. 4(b). Through PWM control, the total variable resistance R_v can be represented as

$$R_v = R_2 + d(R_1//R_{sw}) + (1-d)R_1 \approx R_2 + (1-d)R_1 \quad (8)$$

where R_{sw} denotes the turn-on resistance of the switch which is implemented herein using the CMOS IC *CD*4066 . It is reasonably assumed that $R_{sw} \ll R_1$ in the choice of R_1. The duty ratio of the PWM scheme can be found to be $d = v_c/\hat{V}_{saw}$ with v_c and $\hat{V}_{saw}$ being the control voltage and the amplitude of the sawtooth voltage v_{saw}, respectively. And then, the delay time interval τ_1 of the *SN*74 121 can be expressed as

$$\tau_1 = R_v C \approx \left[\left(1 - \frac{v_c}{\hat{V}_{saw}}\right) R_1 + R_2\right] C \quad (9)$$

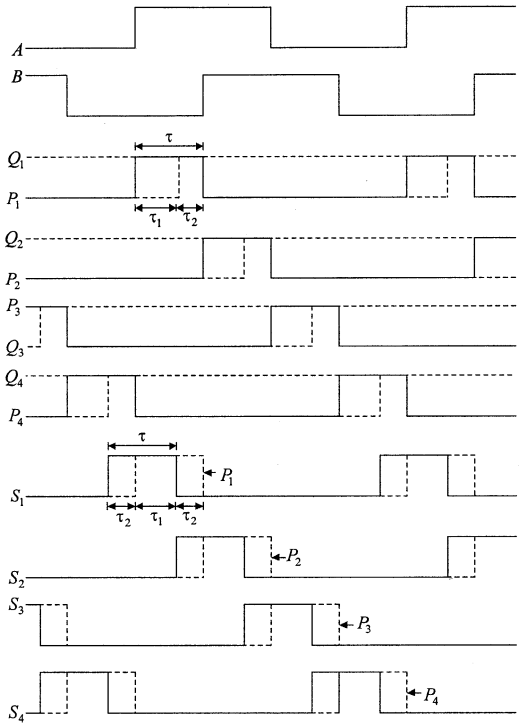

Fig. 5. Typical waveforms used to explain how to generate the modified advancing commutation signals.

From (7) to (9), one can find that the more v_c or d increases, the more R_v decreases, causing τ_1 to decrease, and hence, τ_2 to increase.

D. Experimental Observations

Before the development of the proposed self-tuning control approach to decide the intelligent commutation of the singly excited SRM drive, some experimental observations are made. The operating conditions are described as follows: 1) dc-link voltage V_{dc} is set to 300 V; 2) speed command ω_r^* is chosen to be 5.16 V (1500 r/min); and the motor speed is regulated to be constant using a PI controller $G_{c\omega}(s) = k_{p\omega} + k_{i\omega}/s$ with $k_{p\omega} = 10$ and $k_{i\omega} = 30$; 3) the PI current controller $G_{ci}(s) = k_{pi} + k_{ii}/s$ has $k_{pi} = 75$ and $k_{ii} = 10\,000$; and 4) the load resistance of the dc generator $R_L = 88\,\Omega$. As to the advancing duration τ_2, it is varied from 0.3 to 1.2 ms in steps of 0.15 ms. The measured current commands I_c for different values of advancing duration τ_2 are listed in Table I and plotted in Fig. 6. The results show that there exists a minimum point, which allows the self-tuning control to be possible to achieve.

E. Proposed Self-Tuning Mechanism

1) Dynamic Signal Analysis: From Figs. 4, 5, and the preceding descriptions, it is obvious that tuning the control voltage v_c in the PWM scheme can vary the advancing duration τ_2, and thus, minimum drawn line current is obtained. In order to develop a stable and efficient tuning algorithm, the dynamic signal analysis is first made to observe the relationship between the changes of v_c and I_c. Define

$$\Delta I_c(n) \triangleq I_c(n) - I_c(n-1)$$

current command change at the

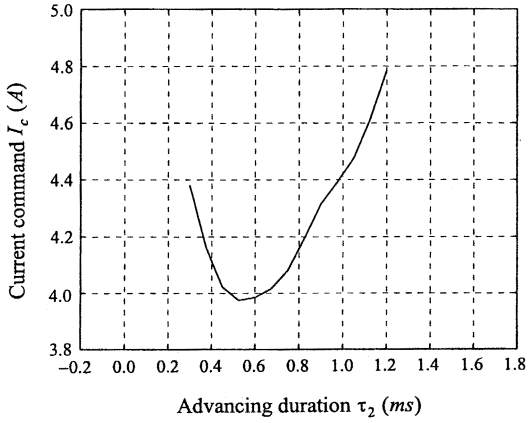

Fig. 6. Measured current commands for different values of advancing duration.

TABLE I
MEASURED CURRENT COMMANDS FOR DIFFERENT VALUES OF ADVANCING DURATION

Advancing duration $\tau_2(ms)$	Current command $I_c(A)$
0.30	4.38
0.45	4.02
0.60	3.99
0.75	4.08
0.90	4.32
1.05	4.48
1.20	4.78

$$\Delta v_c(n) \triangleq v_c(n) - v_c(n-1)$$

nth sampling interval

control voltage change at the

nth sampling interval.

The possible dynamic phenomena of I_c, due to the change of v_c, are sketched in Figs. 7(a)–7(d), which are described as follows.

a) Mode 1: As shown in Fig. 7(a), $\Delta v_c(n) > 0$ and $\Delta I_c(n) < 0$ at the nth sampling interval, which implies that I_c is approaching to the minimum value I_c^*. Hence, $\Delta v_c(n+1)$ at the next sampling interval must be positive to make I_c continuously decrease.

b) Mode 2: As shown in Fig. 7(b), $\Delta v_c(n) > 0$ and $\Delta I_c(n) > 0$ at the nth sampling interval, which indicates that I_c is departing from I_c^*. Thus, at the next sampling interval, $\Delta v_c(n+1)$ must be negative to reduce I_c, thus forcing I_c to approach to I_c^* in the opposite direction.

c) Mode 3: As illustrated in Fig. 7(c), $\Delta v_c(n) < 0$ and $\Delta I_c(n) < 0$ at the nth sample interval, which indicates that I_c is approaching I_c^*. Therefore, $\Delta v_c(n+1)$, at the next sampling interval, must be negative to make I_c continuously decrease.

d) Mode 4: As depicted in Fig. 7(d), $\Delta v_c(n) < 0$ and $\Delta I_c(n) > 0$ at the nth sampling interval, which shows that I_c is departing from I_c^*. Consequently, $\Delta v_c(n+1)$ at the next sampling interval must be positive, thus forcing I_c to move to I_c^* in the opposite direction.

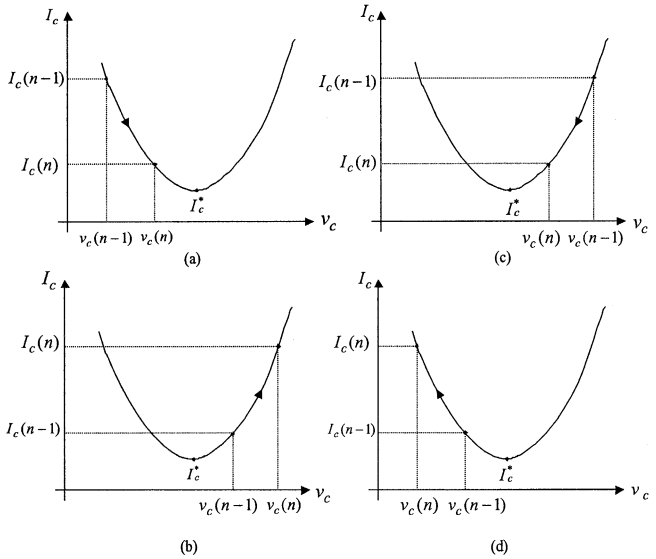

Fig. 7. Dynamic signal analysis of the proposed control approach, (a) to (d): mode 1 to mode 4.

TABLE II
PROPOSED LINGUISTIC TUNING CONTROL ALGORITHM FOR $\Delta v_c(n+1)$

$\Delta I_c(n)$ \ $\Delta v_c(n)$	+	−
+	+ Mode 2	+ Mode 4
−	+ Mode 1	− Mode 3

2) Implementation of Tuning Mechanism: According to the above intuitive analysis, the linguistic tuning algorithms for $\Delta v_c(n+1)$ described before are tabulated in Table II and accordingly, the tuning control law is proposed as

$$v_c(n+1) = v_c(n) + \Delta v_c(n+1) \tag{10}$$

$$\Delta v_c(n+1) = -K\Delta v_c(n) Sign(\Delta I_c(n)) \tag{11}$$

$$Sign(\Delta I_c(n)) \triangleq \begin{cases} 1 : \Delta I_c(n) > 0 \\ -1 : \Delta I_c(n) < 0 \end{cases} \tag{12}$$

where $Sign(\Delta I_c(n))$ is a sign function to obtain the direction of the current command change $\Delta I_c(n)$ and K is a proportional gain employed to adjust the control sensitivity. The implementation of the proposed tuning control scheme is shown in Fig. 8. The discrete variables $v_c(n)$ and $I_c(n)$ are yielded from the continuous ones through the sample and hold (S/H) IC LF398. After determining the updated control voltage $v_c(n+1)$ according to the tuning law from (10)–(12), the new control voltage $v_c(t)$ is obtained through a low-pass filter. The sampling frequency of S/H is chosen to be 10 Hz and the corner frequency of the low-pass filter is chosen as $f_c = 5$ Hz. In the PWM scheme, the frequency and amplitude of the sawtooth wave are set to be 60 kHz and $\hat{V}_{saw} \approx 3.5$ V, respectively. The circuit components of the IC SN74121 shown in Fig. 4(b) are

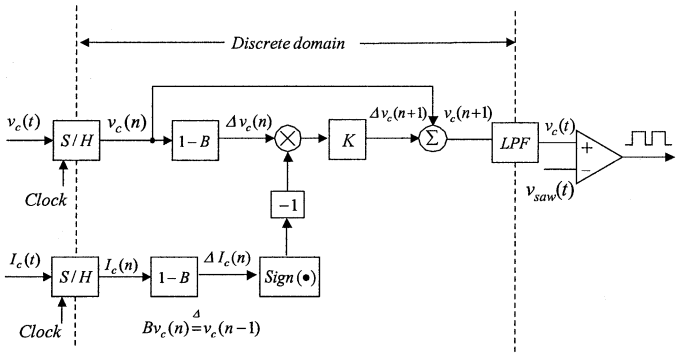

Fig. 8. Configuration of the proposed intelligent self-tuning control mechanism.

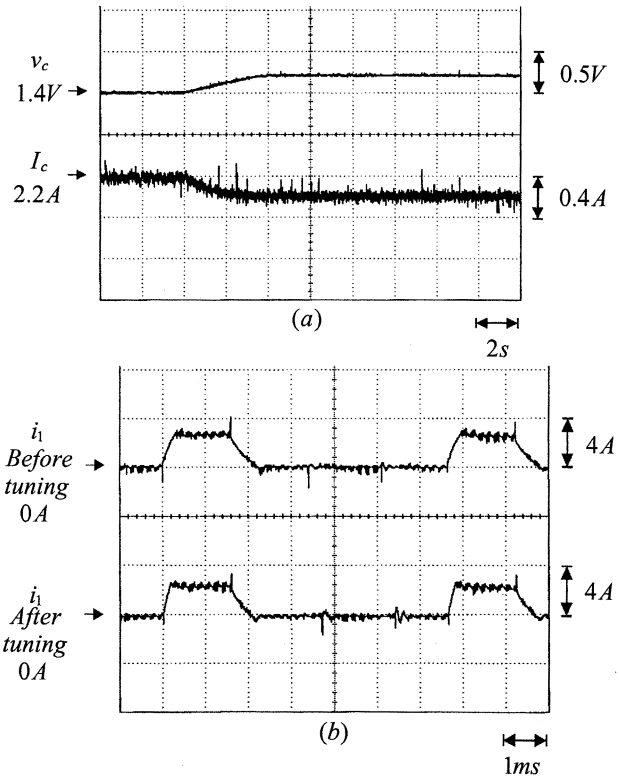

Fig. 9. Measured traces before and after applying the proposed scheme under the load resistance $R_L = \infty\ \Omega$ at 1500 r/min: (a) control voltage v_c and current command I_c; (b) steady-state phase-winding currents.

chosen to be $R_1 = 7.2$ kΩ, $R_2 = 0.35$ kΩ and $C = 1\ \mu$F. The proportional gain of the tuning scheme is set to be $K = 6$.

IV. Experimental Results

Having made the design and implementation of the SRM drive with the proposed commutation tuning scheme shown in Figs. 1, 4, and 8, some measured results are provided to confirm the effectiveness of the proposed control method. Let the motor be stably regulated at 1500 r/min using the controller and system parameters set in Section III. Fig. 9(a) shows the measured control signal v_c and current command I_c before and after the tuning under the load resistance $R_L = \infty\Omega$. The measured dc-link currents I_{dc} are 1.43 and 1.31 A before and after tuning, respectively. Under the same conditions as above, Fig. 9(b) shows the measured phase-winding currents before and after finishing the

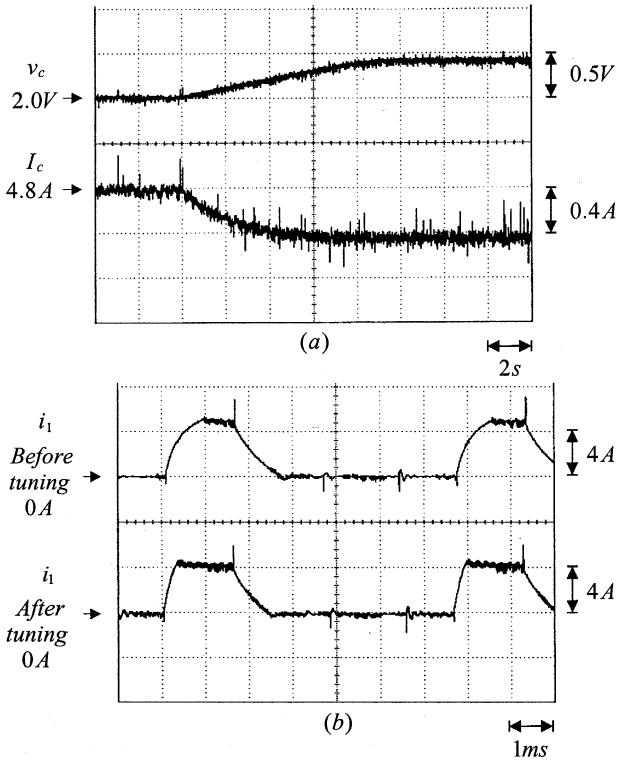

Fig. 10. Measured results before and after applying the proposed tuning scheme under the load resistance $R_L = 57\ \Omega$ at 1500 r/min: (a) control voltage v_c and current command I_c; (b) steady-state phase-winding currents.

tuning. Now let $\omega_r = 1500$ r/min and $R_L = 57\ \Omega$, the measured results similar to those of Figs. 9(a) and 9(b) are plotted in Figs. 10(a) and 10(b). In this case, the dc-link current I_{dc} is decreased from 4.18 A before tuning to 3.65 A after tuning. It is obvious from the results shown in Figs. 9 and 10 that the current commands are reduced by applying the proposed commutation tuning control approach.

In general, for a motor running at a constant speed with a given load, this decrease in required current implies that the torque generating capability is increased. Accordingly, to further test the motor torque generating characteristics using the same speed controller, Figs. 11(a) and 11(b) show the measured speeds due to speed command change of 100 r/min when the motor is running at 1400 r/min and $R_L = 57\ \Omega$, before and after tuning. Figs. 12(a) and 12(b) show the measured speeds due to the step load change from $R_L = 57\ \Omega$ to 34 Ω at 1400 r/min, before and after tuning. The results shown in Figs. 11 and 12 indicate that by employing the proposed tuning approach, the speed tracking response becomes faster and the speed regulation response is also improved in the smaller dip and faster restoration. This is mainly due to the increased torque generating capability of the SRM.

V. Conclusions

The intelligent commutation tuning to yield improved torque generating capability of an SRM has been presented. Initially, the effect of commutation instant change on the torque generating characteristics of the SRM is observed. Then accordingly, an intelligent commutation tuning approach is developed to increase the torque generating capability. In the proposed tuning

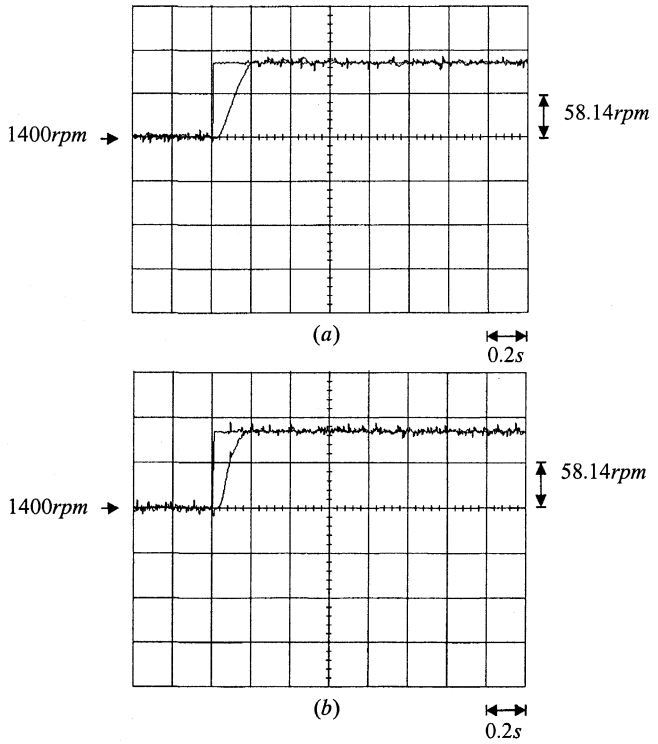

Fig. 11. Measured speed responses due to speed command change (1400 to 1500 r/min at $R_L = 57\ \Omega$): (a) before tuning; (b) after tuning.

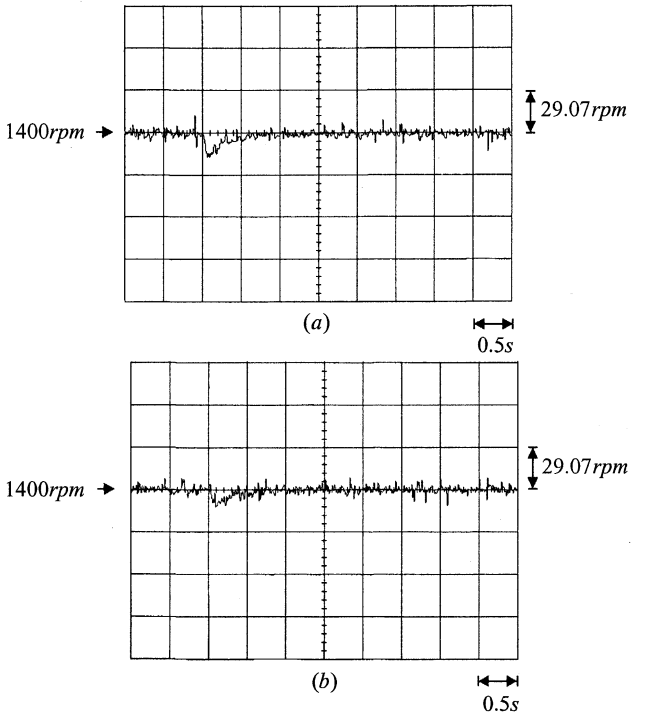

Fig. 12. Measured speed responses due to step load change ($R_L = 57\ \Omega$ to 34 Ω at 1400 r/min): (a) before tuning; (b) after tuning.

scheme, the minimization of the motor drawn line current is employed as a performance index to equivalently yield maximum TPA. Finally, the circuit implementation of the developed tuning scheme is presented. The experimental results indicate that through the proposed appropriate commutation tuning, the motor can draw minimum current under any load condition, which implies that the motor conversion efficiency is considerably upgraded. Besides, the tracking and regulation speed responses are also improved.

REFERENCES

[1] T. J. E. Miller, *Switched Reluctance Motors and Their Control*. Oxford, U.K.: Clarendon Press, 1993.
[2] J. Mahdavi, G. Suresh, B. Fahimi, and M. Ehsani, "Dynamic modeling of nonlinear SRM drive with Pspice," in *IEEE Proc. Ind. Applicat. Conf.*, vol. 1, 1997, pp. 661–667.
[3] H. Le-Huy, P. Viarouge, and B. Francoeur, "A novel unipolar converter for switched reluctance motor," *IEEE Trans. Power Electron.*, vol. 5, pp. 469–475, Oct. 1990.
[4] H. Le-Huy, K. Slimani, and P. Viarouge, "A current-controlled quasiresonant converter for switched-reluctance motor," *IEEE Trans. Ind. Electron.*, vol. 38, pp. 355–362, Oct. 1991.
[5] Y. G. Dessouky, B. W. Williams, and J. E. Fletcher, "A novel power converter with voltage-boosting capacitors for a four-phase SRM drive," *IEEE Trans. Ind. Electron.*, vol. 45, pp. 815–823, Oct. 1998.
[6] K. I. Hwu and C. M. Liaw, "DC-link voltage boosting and switching control for switched reluctance motor drives," *Proc. Inst. Elect. Eng.—Elect. Power Applicat.*, vol. 147, pp. 337–344, 2000.
[7] D. A. Torrey and J. H. Lang, "Optimal-efficiency excitation of variable-reluctance motor drives," *Proc. Inst. Elect. Eng.*, pt. B, vol. 138, no. 1, pp. 1–14, 1991.
[8] D. S. Reay, T. C. Green, and B. W. Williams, "Minimization of torque ripple in a switched reluctance motor using a neural network," in *IEEE Proc. Int. Artificial Neural Networks Conf.*, 1993, pp. 224–228.
[9] I. Husain and M. Ehsani, "Torque ripple minimization in switched reluctance motor drives by PWM current control," *IEEE Trans. Power Electron.*, vol. 11, pp. 83–88, Jan. 1996.
[10] H. C. Lovatt and J. M. Stephenson, "Computer-optimized smooth-torque current waveforms for switched-reluctance motors," *Proc. Inst. Elect. Eng. —Elect. Power Applicat.*, vol. 141, no. 2, pp. 45–51, 1994.
[11] M. Ehsani and K. R. Ramani, "Direct control strategies based on sensing inductance in switched reluctance motors," *IEEE Trans. Power Electron.*, vol. 11, pp. 74–82, Jan. 1996.
[12] P. C. Kjaer, P. Nielsen, L. Andersen, and F. Blaabjerg, "A new energy optimizing control strategy for switched reluctance motors," *IEEE Trans. Ind. Applicat.*, vol. 31, pp. 1088–1095, Sept./Oct. 1995.
[13] P. Tandon, A. V. Rajarathnam, and M. Ehsani, "Self-tuning control of a switched-reluctance motor drive with shaft position sensor," *IEEE Trans. Ind. Applicat.*, vol. 33, pp. 1002–1010, July/Aug. 1997.
[14] A. V. Rajarathnam, B. Fahimi, and M. Ehsani, "Neural network based self-tuning control of a switched reluctance motor drive to maximize torque per ampere," in *IEEE Proc. Ind. Applicat. Soc. Conf.*, vol. 1, 1997, pp. 548–555.
[15] B. Fahimi, G. Suresh, J. P. Johnson, M. Ehsani, M. Arefeen, and I. Panahi, "Self-tuning control of switched reluctance motors for optimized torque per ampere at all operating points," in *IEEE Proc. Appl. Power Electron. Conf.*, vol. 2, 1998, pp. 778–783.
[16] K. Russa, I. Husain, and M. Elbuluk, "A self-tuning controller for switched reluctance machines," in *IEEE Proc. Power Electron. Specialists Conf.*, vol. 2, 1998, pp. 1269–1275.

K. I. Hwu was born in Taiching, Taiwan, R.O.C., on August 24, 1965. He received the B.S.E.E. and Ph.D. degrees from National Tsing Hua University, Hsinchu, Taiwan, R.O.C., in 1996 and 2001, respectively.

His areas of research interest are power electronics and motor drives.

C. M. Liaw (S'88-M'89) was born in Taiching, Taiwan, R.O.C., on June 19, 1951. He received the B.S. degree in electronic engineering from the evening department at Tamkang College of Arts and Sciences, Taipei, Taiwan, R.O.C., in 1979, and the M.S. and Ph.D. degrees in electrical engineering from National Tsing Hua University, Hsinchu, Taiwan, R.O.C., in 1981 and 1988, respectively.

Currently, he is a Professor in the Department of Electrical Engineering. In 1988, he joined the faculty of National Tsing Hua University as an Associate Professor in electrical engineering. His areas of research interest are power electronics, motor drives, and electric machine control.

Dr. Liaw is a life member of the CIEE.